AIAA JOURNAL
Vol. 36, No. 2, February 1998

Prediction of Viscous Trailing Vortex Structure from Basic Loading Parameters

John A. Rule* and Donald B. Bliss†
Duke University, Durham, North Carolina 27708

An analytical method has been developed to predict the structure of a fully developed trailing vortex with a viscous core. Vortex structure is calculated from the load distribution on the generating wing and fundamental conservation laws are satisfied. The present rollup model implicitly addresses viscous effects in the vortex core region by assuming a turbulent mixing process in the core during formation. Mixing theory suggests the appropriate functional form of the solution velocity profiles within this region, with constants that are determined uniquely by the method for arbitrary wing loading distributions. Important structural properties such as vortex strength, core size, and peak swirl velocity are calculated directly from these solution constants. The viscous core model was validated against two recent experimental studies, which provided new insight into vortex growth.

Nomenclature

A_1	= shooting parameter
C_L	= coefficient of lift
F_1, F_2, G_1, G_2	= auxiliary functions
m	= core axial velocity power law
p	= pressure
p_∞	= freestream pressure
R	= core radius ratio, r_s/r_t
r	= vortex radius
r_c	= vortex outer radius: complete inviscid rollup
r_{in}	= streamtube inlet radius
r_p	= vortex outer radius: partial inviscid rollup
r_s	= solid body region outer radius
r_t	= turbulent core radius
s	= span of rollup region (wing semispan)
U_∞	= freestream velocity
u	= vortex axial velocity
v	= vortex swirl velocity
α	= wing geometric angle of attack
Γ	= bound circulation
$\Gamma_{\max}$	= maximum bound circulation
$\tilde{\Gamma}$	= vortex circulation
ϵ	= dimensionless wing loading strength
ξ	= spanwise coordinate (from tip)
$\bar{\xi}$	= centroid of vorticity

Subscripts and Superscript

i	= initial condition
t	= value on turbulent core boundary
$\hat{}$	= dimensionless quantity

Introduction

A CONSEQUENCE of lift on any finite wing is the presence of well-organized downstream trailing vortices. These vortices are produced by rollup of the unstable trailing vortex sheet produced by changes in the bound vorticity along the wing span. Trailing vortex formation has been a problem of interest for some time, due to the hazard posed by the swirling wake of large aircraft to smaller following aircraft.[1–9] More recently, blade-tip trailing vortex structure has been found to be critical to the accurate calculation of blade–vortex interaction (BVI) noise in rotorcraft aeroacoustics.[10–16] Trailing vortex formation has been examined both experimentally[17–25] and computationally.[26–28]

The theoretical basis for the present vortex model lies with the Betz method for vortex sheet rollup,[29] which relates circulation in an axisymmetric trailing vortex to bound circulation on a generating wing. Previous extensions to the Betz model include the allowance for axial flow in a fully developed vortex[1] and a set of criteria to determine when multiple vortices will be shed from a single body.[7] A differential formulation of vortex rollup has provided some insight into the coherent spiral structure of a trailing vortex during formation.[30]

Previous rollup models based on the Betz method suffered from the shortcoming of singular velocities in the center, or core region, of the predicted vortex. These singularities result from two factors: singular vorticity at the outboard edge of the initial vortex sheet for most cases of interest and the assumption that the rollup process is completely inviscid. Away from the core region, the inviscid assumption was shown to be valid,[5] which suggests that viscous effects can be treated locally in the core.

Fully developed vortices seem to exhibit rather simple functional behavior within the core, which has led to the common use of the Scully algebraic core model.[31] Whereas this model often provides a good fit to experimental data, it is generally necessary to adjust the total circulation and core size for every configuration of interest. This limits the model to use only for fitting data but precludes the ability to predict vortex structure.

To date, no general method has been developed to accurately relate downstream viscous trailing vortex structure and strength to loading conditions on the generating wing. The present paper develops a new method that applies fundamental conservation laws to the problem of vortex sheet rollup and uniquely determines downstream trailing vortex properties from arbitrary upstream wing loading conditions. This general method was developed for fixed-wing rollup but can readily be applied to rotor blade tip rollup because rollup of the vortex core region typically occurs over a short length scale, in which case wake curvature effects are negligible.

The present work extends the three-dimensional inviscid Betz type model to allow for a viscous core. Integral conservation laws similar to those used in inviscid rollup theory are applied to a portion of the bound circulation at the tip of a wing. Upon leaving the wing, the outboard edge of the trailed sheet of vorticity undergoes turbulent mixing, forming a core that exhibits prescribed functional behavior for both swirl and axial velocity. These prescribed velocity profiles contain several unknown constants that are uniquely determined by satisfying the integral conservation laws. By this formulation, viscous effects within the core are treated implicitly. The remainder of the trailed vorticity sheet rolls up around the viscous core according to the inviscid differential rollup relations.

Presented as Paper 96-2495 at the AIAA 14th Applied Aerodynamics Conference, New Orleans, LA, June 17–20, 1996; received March 5, 1997; revision received Sept. 15, 1997; accepted for publication Oct. 10, 1997. Copyright © 1997 by John A. Rule and Donald B. Bliss. Published by the American Institute of Aeronautics and Astronautics, Inc., with permission.

*Research Assistant, Department of Mechanical Engineering and Materials Science, Box 90302. E-mail: jarule@duke.edu. Member AIAA.

†Associate Professor, Department of Mechanical Engineering and Materials Science, Box 90300. Member AIAA.

The method does not address the effects of dissipation or decay, but does provide the correct vortex core structure immediately downstream of the generating span. This new formulation contains no free parameters, eliminating the need to arbitrarily assign a core radius or circulation to the predicted vortex.

Inviscid Vortex Model

The viscous trailing vortex model developed in this paper makes use of a new, three-dimensional, differential formulation relating the known bound circulation on a generating wing to axial and swirl velocity in a fully developed downstream trailing vortex. This formulation begins with a set of assumptions first suggested by Betz,[29] which are briefly reviewed next.

The original Betz vortex model applies to an inviscid, incompressible, two-dimensional unbounded flow. By examining the time invariants of the flow, Betz showed that a system of discrete vortices will maintain a constant total circulation, centroid of vorticity, and second moment of vorticity under the assumption of no externally applied forces. This is analogous to the behavior of a system of discrete masses, which have a fixed total mass, centroid, and second moment relative to a fixed coordinate system.

This argument can readily be extended to a sheet of distributed vorticity, conserving circulation, centroid of vorticity, and second moment of vorticity on a station-by-station basis throughout the rollup process. All properties are conserved between the rolled up portion of the sheet and an axisymmetric vortex of unknown radius. (See Fig. 1 for a schematic diagram of this incremental rollup process.)

The first integral invariant law, which relates wing bound circulation to vortex circulation,

$$\Gamma(\xi) = \int_0^{\xi} \frac{d\Gamma(\eta)}{d\eta}\, d\eta = \int_0^{r} \frac{d\tilde{\Gamma}(\lambda)}{d\lambda}\, d\lambda = \tilde{\Gamma}(r) \tag{1}$$

is a statement of Kelvin's theorem because for each span location there is a corresponding radial location in the trailing vortex that has that same circulation. Note that the spanwise coordinate system employed here is opposite that usually used in Betz-type analyses.[1,7,30] However, this convention naturally emphasizes the physical relationship between the wingtip, $\xi = 0$, and the center of the vortex, $r = 0$, and preserves the temporal order of the rollup process.

The second integral invariant, centroid of vorticity, is defined in terms of the initial flat sheet circulation by

$$\bar{\xi}(\xi) = \frac{1}{\Gamma(\xi)} \int_0^{\xi} \frac{d\Gamma(\eta)}{d\eta}\, \eta\, d\eta \tag{2}$$

and this centroid determines the location of the center of the resulting axisymmetric vortex.

The final integral invariant, which is the second moment of vorticity, makes use of Eq. (2) by defining the moment arm on the flat sheet as the distance between the point of evaluation and the (fixed) centroid location

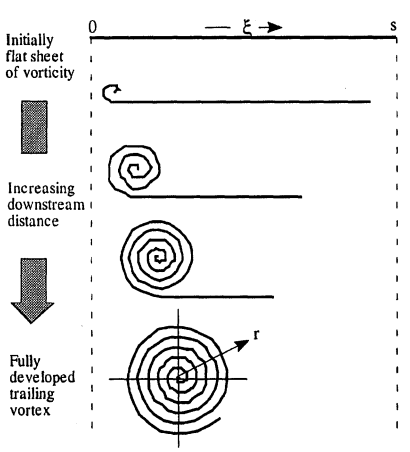

Fig. 1 Schematic diagram of vortex sheet rollup.

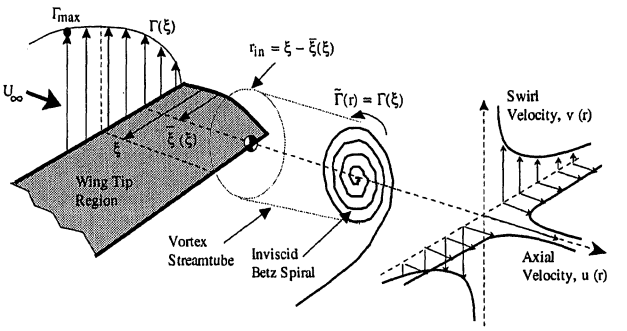

Fig. 2 Geometry of inviscid vortex spiral rollup.

$$\int_0^{\xi} \frac{d\Gamma(\eta)}{d\eta}[\eta - \bar{\xi}(\xi)]^2\, d\eta = \int_0^{r} \frac{d\tilde{\Gamma}(\lambda)}{d\lambda}\lambda^2\, d\lambda \tag{3}$$

Equations (1–3) taken together provide enough information to solve for the relationship between span location and vortex radius, and several authors have shown the following simple result[1,4,7]:

$$r = \xi - \bar{\xi}(\xi) \tag{4}$$

which states that the bound circulation lying between 0 and ξ on the flat sheet is found within radius r in the vortex. Swirl velocity in the vortex is given by

$$v(r) = \frac{\tilde{\Gamma}(r)}{2\pi r} \tag{5}$$

where $\tilde{\Gamma}(r)$ and r are related back to span location ξ by Eqs. (1) and (4), respectively. Note particularly that the station-by-station assumption implies that the sheet can be considered at any intermediate step, not just at the endpoints.

Integration of Eq. (3) by parts yields a more physically meaningful expression:

$$\int_0^{\xi} \rho U_\infty \Gamma(\eta)[\eta - \bar{\xi}(\xi)]\, d\eta = \int_0^{r} \rho U_\infty \tilde{\Gamma}(\lambda)\lambda\, d\lambda \tag{6}$$

which indicates that axial flux of angular momentum is conserved during the vortex rollup process. The left-hand side of Eq. (6) suggests that a torque due to the Kutta–Joukowski lift force is applied to the fluid by the wing, and this torque is directly related to the angular momentum of the downstream vortex. Inviscid spiral rollup behind a wing tip is shown in Fig. 2. Note the geometric relationship between span location, bound circulation, and trailing vortex size and location.

Differential Formulation for Vortex Rollup

Several authors have modified the two-dimensional Betz method to account for axial flow.[4,30] The present work extends the Betz method to provide a differential formulation for inviscid vortex rollup.

Extension of vortex sheet rollup to three dimensions requires slight modification of the preceding equation. Conservation of axial flux of angular momentum for a three-dimensional flow must include nonuniform axial velocity in the downstream vortex:

$$\int_0^{\xi} \rho U_\infty \Gamma(\eta)[\eta - \bar{\xi}(\xi)]\, d\eta = 2\pi\rho \int_0^{r} u(\lambda)v(\lambda)\lambda^2\, d\lambda \tag{7}$$

When Eq. (7) is reexpressed in differential form:

$$U_\infty 2\pi(\xi - \bar{\xi})\, d(\xi - \bar{\xi}) = u(r)2\pi r\, dr \tag{8}$$

it yields a statement of mass conservation during the rollup process, such that all of the material passing through a circle of radius $(\xi - \bar{\xi})$ at the trailing edge of the wing must be found within a circle of radius r in the vortex, suggesting that the rollup process be considered as taking place on a series of nested, contracting circular stream surfaces. That interpretation will be made here, and this relationship will be emphasized by defining the vortex streamtube inlet radius as

$$r_{\text{in}}(\xi) = \xi - \bar{\xi}(\xi) \tag{9}$$

Note that this inlet radius is the same as that found from the two-dimensional Betz analysis, given by Eq. (4). With the addition of the unknown vortex axial velocity introduced in Eq. (7), this system requires another equation to produce a unique solution. This new equation follows from the initial assumption that the original flat sheet of vorticity rolls up in an orderly fashion into a discrete spiral structure. Each layer of the spiral is separated from the next by a thin layer of inviscid fluid, such that any point in the fluid can be reached without crossing vortex lines during rollup. Thus, Bernoulli's equation applies at all points within the inviscid spiral:

$$p_\infty + \tfrac{1}{2}\rho U_\infty^2 = p(r) + \tfrac{1}{2}\rho[u(r)^2 + v(r)^2] \tag{10}$$

The recognition that Bernoulli's equation applies within the spiral was first made by Batchelor,[32] though that viewpoint did not gain wide acceptance.

The pressure within the vortex is an additional unknown, and so one final equation is necessary to close the system. This equation is obtained by making a radial momentum balance within the vortex, assuming the spiral is essentially axisymmetric, with no radial component of velocity:

$$\frac{1}{\rho}\frac{\mathrm{d}p}{\mathrm{d}r} = \frac{v(r)^2}{r} \tag{11}$$

Eliminating pressure between Eqs. (10) and (11) and using Eq. (5) to express swirl velocity in terms of circulation yields a second differential equation:

$$\mathrm{d}[u(r)^2] = -\frac{1}{4\pi^2 r^2}\,\mathrm{d}[\tilde{\Gamma}(r)^2] \tag{12}$$

relating axial velocity to circulation in the vortex.

The goal of this inviscid analysis was to determine the relationship between wing loading distribution and trailing vortex swirl and axial velocity distributions. Equations (8) and (12) provide this relationship in the form of a pair of coupled, nonlinear, ordinary differential equations (ODEs), which relate the unknown vortex radius and axial velocity to the prescribed wing loading distribution. To aid in the solution of this system, these two ODEs can be rewritten in dimensionless form. For this analysis, all lengths are normalized by the span of the rollup region, all velocities by the freestream velocity, and the circulation by the maximum bound circulation. The dimensionless rollup equations are then

$$\frac{\mathrm{d}\hat{r}^2}{\mathrm{d}\hat{\xi}} = \frac{1}{\hat{u}}\frac{\mathrm{d}\hat{r}_{\mathrm{in}}(\hat{\xi})^2}{\mathrm{d}\hat{\xi}} \tag{13}$$

$$\frac{\mathrm{d}\hat{u}^2}{\mathrm{d}\hat{\xi}} = -\frac{\epsilon^2}{\hat{r}^2}\frac{\mathrm{d}\hat{\Gamma}(\hat{\xi})^2}{\mathrm{d}\hat{\xi}} \tag{14}$$

where a new dimensionless parameter,

$$\epsilon \equiv \frac{\Gamma_{\max}}{2\pi s U_\infty} \propto \frac{C_L}{\mathrm{AR}} \tag{15}$$

has been defined. Typically, ϵ is of order 0.01. Note that all quantities are now expressed parametrically in terms of the dimensionless wing span location $\hat{\xi}$.

This system of Eqs. (13) and (14) must be solved subject to the following set of physically imposed boundary conditions: The center of the vortex ($\hat{r} = 0$) corresponds to the outboard edge of the vortex sheet ($\hat{\xi} = 0$), the outer edge of the vortex ($\hat{r} = \hat{r}_c$) corresponds to the inboard edge of the vortex sheet ($\hat{\xi} = 1$), and the axial velocity returns to the freestream value ($\hat{u} = 1$) at the outer edge of the vortex.

In general, the governing equations must be numerically integrated, which involves a shooting problem to satisfy the axial velocity boundary condition. Difficulty arises in the solution of the rollup equations because a set of three initial conditions, $\hat{\xi}_i$, $\hat{r}_i$, and $\hat{u}_i$, are necessary to start the numerical integration. Because velocity is singular exactly at the wing tip, a local power series solution to the governing equations, valid only near the tip, must be found to provide the correct mathematical relationships between the three initial conditions. Determining these relationships is not a trivial matter due to the nature of the nonlinearity in the governing equations, and the details of that procedure are discussed in the Appendix. For the case of elliptic loading, the local tip solution is

$$\begin{aligned}\hat{u}_i &= (27/8)\epsilon^2\hat{\xi}_i^{-1}\left(1 + A_1\hat{\xi}_i^{(\sqrt{13}-1)/2} + \cdots\right)\\ \hat{r}_i &= (8/27\epsilon)\hat{\xi}_i^{\frac{3}{2}}\left(1 - 0.348612A_1\hat{\xi}_i^{(\sqrt{13}-1)/2} + \cdots\right)\end{aligned} \tag{16}$$

where the shooting parameter A_1 is adjusted to satisfy the outer boundary condition. Using these starting conditions, the coupled rollup equations were numerically integrated using a fourth-order accurate Runge–Kutta scheme in conjunction with very small increments of $\hat{\xi}$.

Inviscid Rollup Results

Core swirl and axial velocity were calculated for the case of inviscid rollup behind an elliptically loaded wing. These results are shown in Figs. 3 and 4, respectively, on both a normal scale and a radially expanded scale, which shows more clearly the behavior in the core region. For comparison, the same calculations were made for classical two-dimensional Betz rollup. Except for the region very near the center of the vortex, the present three-dimensional model gives results very similar to the Betz model. However, the local tip solution of Eq. (16) demonstrates that $u \propto r^{-2/3}$. It can be shown that $v \propto r^{-2/3}$ as well. This is a stronger singularity than that predicted by classical Betz theory, which finds $v \propto r^{-1/2}$. The stronger singularity occurs because the presence of axial flow causes a radial contraction and intensification of the vortex core. Note that inviscid rollup always produces an axial velocity excess, which occurs in a region roughly comparable to that often associated with viscous effects in experimental measurements.

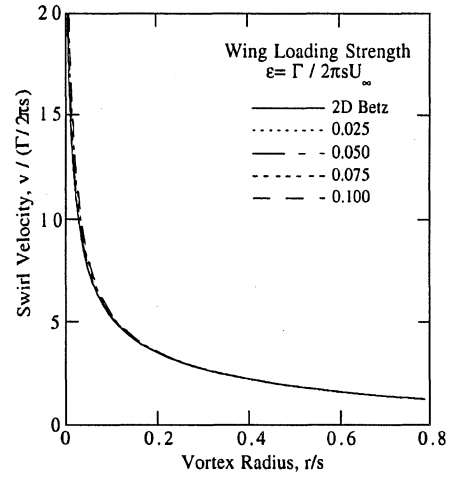

Normal scale

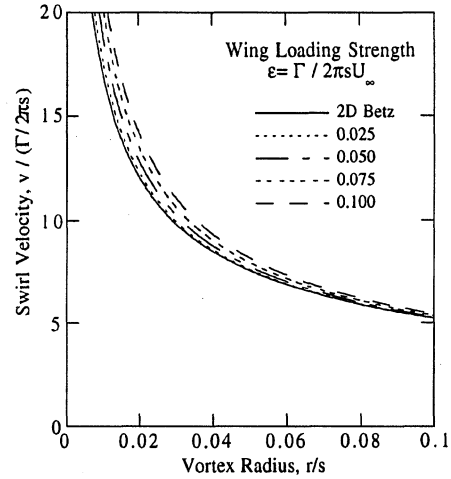

Expanded scale

Fig. 3 Vortex swirl velocity.

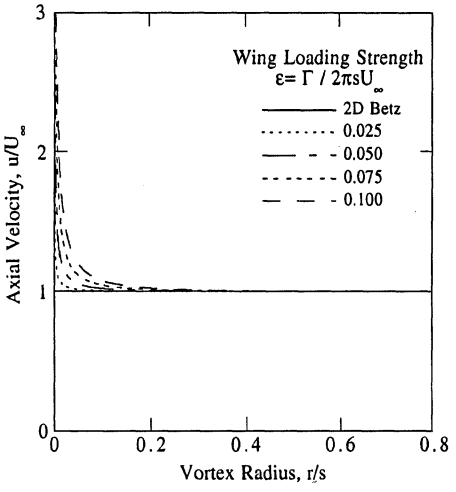

Normal scale

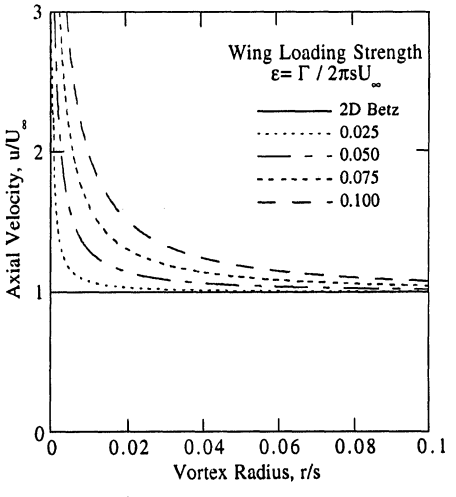

Expanded scale

Fig. 4 Vortex axial velocity.

Viscous Core Model

Overview

The preceding inviscid vortex rollup model predicts singular swirl and axial velocities in the vortex core for all practical load distributions due to the inviscid nature of the model. In reality, viscous effects will adjust the flow in the center of the vortex, resulting in smooth, bounded velocity distributions.

The following viscous vortex model makes use of the inviscid rollup formulation, with the exception that the inviscid spiral structure no longer extends to the center of the vortex. Instead, one of the nested streamtubes postulated in the inviscid model is assumed to act as a viscous core boundary, dividing the vortex into an inner viscous core region and an outer inviscid spiral. Within this dividing streamtube, turbulent mixing occurs during rollup, removing the swirl and axial velocity singularities while still satisfying the rollup conservation laws. This concept is shown in Fig. 5, which differs from Fig. 2 only in the inclusion of the turbulent core streamtube.

Within the viscous core, fundamental properties (mass flux, axial flux of angular momentum, and axial momentum flux) are conserved in an integral sense between the initial sheet of trailed vorticity and the downstream trailing vortex. Recall that a similar, more restrictive set of conservation laws was applied on a station-by-station basis throughout the vortex for purely inviscid rollup. Swirl and axial velocity in the downstream viscous core assume prescribed functional forms with undetermined constants, in a spirit similar to the Karman–Pohlhausen method for boundary layers.[33] Outside the viscous core, the inviscid spiral structure of the preceding section applies.

This combination of integral conservation laws and inviscid differential rollup equations reduces to a system of two coupled, nonlinear ODEs and three nonlinear algebraic equations, all of which

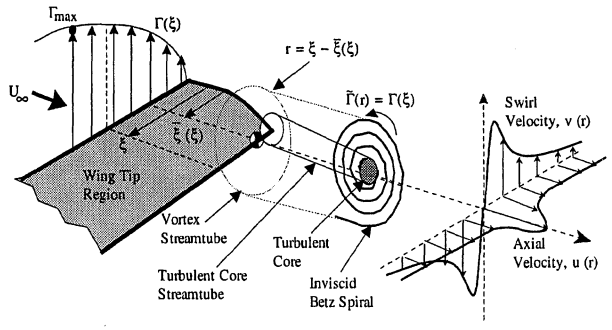

Fig. 5 Turbulent core formation within inviscid spiral.

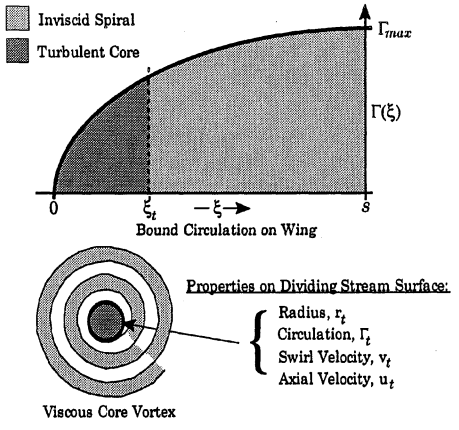

Fig. 6 Bound circulation is divided between the turbulent core and surrounding inviscid spiral.

must be satisfied simultaneously. The undetermined constants serve as solution parameters to the governing system of conservation equations. All equations can be expressed in closed form, but numerical solution of the system is required due to the nonlinear nature of the equations. A unique set of solution parameters exists for each wing loading strength and load distribution.

Determination of the span location and corresponding streamtube that divide the viscous core and inviscid spiral regions, and consequently the radial location, or core radius, of the viscous core boundary in the vortex, is the primary result of this work. The bound circulation associated with the initial flat sheet of vorticity is also divided between the viscous core and the surrounding inviscid spiral, as shown in Fig. 6.

Viscous Core Structure

Some freedom exists when selecting the functional forms of the viscous core velocity distributions; however, previous analyses and experiments have found repeatable trends in vortex core properties, suggesting the use of the following functions.

Swirl velocity distributions were chosen to be consistent with a turbulent mixing model first applied to vortices by Hoffmann and Joubert.[24] Following the mixing length theory of Prandtl, these authors demonstrated that a concentrically circular flow with viscosity will have a region where circulation is proportional to the logarithm of radius. This region is characterized by inertial forces, which are small compared to Reynolds stresses, and will contain the point of maximum swirl velocity. The presence of this logarithmic transition region has been experimentally confirmed by several researchers.[20,22,24,34]

The logarithmic transition region is crucial to the present viscous core model, because it provides a mechanism for including the effects of viscosity in the vortex rollup process, without explicitly requiring the inclusion of an arbitrary eddy viscosity, mixing length, or core radius. Instead, the fully developed trailing vortex is assumed to have velocity profiles consistent with turbulent mixing, and the vortex conservation laws derived in the following section determine uniquely the constants associated with these functional forms.

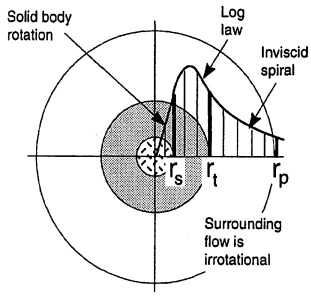

Fig. 7 Swirl velocity distribution in the turbulent core model vortex.

Physical arguments require that, inside the annular logarithmic region, the flow must behave like solid body rotation, so that swirl velocity is zero at the center of the vortex and shear stress is minimized. Outside the logarithmic region, the flow is nearly inviscid, and another mechanism will govern the flow. The present work assumes that the outer inviscid region is governed by the rollup model derived in the preceding section.

Following the stated arguments, the viscous core swirl velocity was defined in a piecewise continuous fashion:

$$v(r) = \begin{cases} ar & 0 < r < r_s \\ (1/r)(b + c\,\ell_n r) & r_s < r < r_t \end{cases} \tag{17}$$

where the three constants a, b, and c are not the undetermined constants mentioned earlier but are used to satisfy three continuity conditions in the core: value and slope at r_s and value at r_t. After satisfying these requirements, the two-region core swirl velocity is

$$v(r) = \left(\frac{v_t}{1 + 2\,\ell_n(r_t/r_s)}\right) \times \begin{cases} \left(\dfrac{r_t}{r_s}\right)\left(\dfrac{r}{r_s}\right) & 0 < r < r_s \\ \left(\dfrac{r_t}{r}\right)\left(1 + 2\,\ell_n \dfrac{r}{r_s}\right) & r_s < r < r_t \end{cases} \tag{18}$$

These two regions taken together will be referred to as the turbulent core and r_t as the turbulent core radius. This terminology was chosen to emphasize that the primary mechanism within this radius during core formation is turbulent mixing due to viscosity. Note that no distinction between laminar and turbulent vortices based on Reynolds number is made in this model. The two radii, r_s and r_t, in Eq. (18) are the second and third of four undetermined constants, which will be found during the solution procedure.

Swirl velocity in the outer inviscid spiral region is governed by the coupled differential rollup equations developed in the preceding section and is calculated using Eq. (5). (See Fig. 7 for a schematic diagram of the assumed swirl velocity distribution in the viscous vortex.)

The choice of axial velocity within the turbulent core is more arbitrary because there seems to be no clearly observed relationship between wing loading and downstream core axial velocity. In general, heavier loading results in an axial velocity excess (greater than freestream velocity), whereas lighter loading produces a mild deficit.[17,18,21] Increasing drag on the generating span has been shown to produce a larger axial velocity deficit.[17,18] Unfortunately, many experimental vortex studies have concentrated only on measuring core swirl velocity, leaving axial velocity unreported. Regardless of this, the exact modeling of the functional form of the axial velocity is considered here to be less important than the recognition that rollup is a three-dimensional process and requires a reasonable axial velocity assumption to accurately model the flow physics.

With these facts in mind, a two-region axial velocity function is constructed in a manner similar to the swirl velocity function:

$$u(r) = \begin{cases} d + e(r/r_s)^2 & 0 < r < r_s \\ f + g(r/r_t)^m & r_s < r < r_t \end{cases} \tag{19}$$

where the four constants d, e, f, and g are used to satisfy four axial velocity continuity conditions. The first three conditions, continuous value and slope at r_s and value at r_t, are identical to those for swirl velocity. The fourth comes from satisfying continuity in the turbulent core streamtube, with inlet radius given by Eq. (9) and uniform freestream inlet velocity:

$$\int_0^{r_{\text{in}}} \rho\, U_\infty\, 2\pi r\, \mathrm{d}r = \int_0^{r_t} \rho u(r)\, 2\pi r\, \mathrm{d}r \tag{20}$$

The parameter m, introduced in Eq. (17), provides the ability to examine the effect of assuming different power laws in the core region. Ideally, this parameter should be chosen based on measured vortex data and is not considered to be a free parameter. After satisfying the four continuity conditions, the core axial function becomes

$$u(r) = u_t + \frac{4(m+2)\left[U_\infty (r_{\text{in}}/r_t)^2 - u_t\right]}{m\left[4 + (m-2)(r_s/r_t)^{2+m}\right]} \times \begin{cases} 1 - \left(\dfrac{r_s}{r_t}\right)^m \left[\dfrac{2-m}{2} + \dfrac{m}{2}\left(\dfrac{r}{r_s}\right)^2\right] & 0 < r < r_s \\ 1 - \left(\dfrac{r}{r_t}\right)^m & r_s < r < r_t \end{cases} \tag{21}$$

where u_t is the fourth and final undetermined solution parameter.

Viscous Core Conservation Laws

A complete set of vortex core velocity functions has been defined, with an accompanying set of four undetermined solution parameters: ξ_t, the span location that divides the bound circulation between turbulent core and inviscid spiral; r_s, the outer radius of the solid body rotation region; r_t, the outer radius of the logarithmic region; and u_t, the axial velocity at the turbulent core boundary. A set of four constraints is required to close the system and produce a unique set of solution parameters.

The first constraint is provided by the coupled differential rollup equations (13) and (14). By assumption, the portion of the vortex sheet outside the turbulent core will roll up around the core in accordance with the inviscid rollup equations in such a manner that the outer boundary condition of freestream axial velocity is satisfied. Unlike the case of completely inviscid rollup, however, the initial conditions required to start the integration are the values of ξ, r, and u on the turbulent core dividing streamtube; by definition these values are ξ_t, r_t, and u_t. The numerical shooting problem still exists, which in practice entails fixing two of the three parameters and adjusting the third until the outer boundary condition is met. Because of the coupling between the two rollup equations, they impose only one constraint on the system.

The second constraint equation is obtained by conserving axial flux of angular momentum within the turbulent core on an integral basis. Recall that this quantity is conserved on a differential basis in the inviscid spiral, which is a more restrictive condition. Referring back to the integral form of the axial flux of angular momentum equation (7), and normalizing all quantities as before, this equation can be rewritten for the turbulent core as

$$\int_0^{\hat{\xi}_t} \hat{\Gamma}(\eta)\left[\eta - \hat{\xi}(\hat{\xi}_t)\right] \mathrm{d}\eta = \frac{1}{\epsilon} \int_0^{\hat{r}_t} \hat{u}(r)\, \hat{v}(r)\, r^2\, \mathrm{d}r \tag{22}$$

where $u(r)$ and $v(r)$ are defined by Eqs. (21) and (18), respectively. The left-hand side of Eq. (22) contains functions that are prescribed by the particular wing loading under consideration and must be integrated for each case. The right-hand side is dependent only on the choice of viscous core velocity functions and only needs to be evaluated once, analytically. Note that the piecewise continuous definitions of axial and swirl velocity in the core necessitate that the right-hand-side integral be evaluated over two ranges, from 0 to $\hat{r}_s$ and from $\hat{r}_s$ to $\hat{r}_t$. For the present model, this equation becomes

$$\int_0^{\hat{\xi}_t} \hat{\Gamma}(\eta)[\eta - \hat{\xi}(\hat{\xi}_t)]\, \mathrm{d}\eta = \hat{\Gamma}_t \left[\hat{r}_{\text{in}}(\hat{\xi}_t)^2 F_1\left(\frac{r_s}{r_t}, m\right) + \hat{u}_t\, \hat{r}_t^2\, F_2\left(\frac{r_s}{r_t}, m\right)\right] \tag{23}$$

where two new functions, F_1 and F_2, are functions only of the quantity r_s/r_t and m. Because r_s/r_t appears frequently, it is convenient to define a new solution parameter, $R \equiv r_s/r_t$, which replaces r_s as the fourth solution parameter. Physically, R represents the proportion of the viscous core that is strictly solid body rotation and is guaranteed to lie between 0 and 1. Using this new definition, the functions F_1 and F_2 are

$$F_1(R,m) \equiv \frac{R^{2+m}[m^2(m-2)+4(m-6)]+6(m+2)^2R^2-24m[1+(m+2)\,\ell_\nu R]}{6m(m+2)[4+(m-2)R^{2+m}](1-2\,\ell_\nu R)}$$

$$F_2(R,m) \equiv \frac{1}{4}\left(\frac{R^2-4\,\ell_\nu R}{1-2\,\ell_\nu R}\right) - F_1(R,m) \tag{24}$$

Note that different assumptions about viscous core velocity will generally produce an equation with the same form as Eq. (23) but different forms of the functions F_1 and F_2.

The third relationship between the solution parameters is obtained by conserving axial momentum flux across the entire vortex in a manner similar to the preceding conservation of axial flux of angular momentum. The assumed turbulent core velocity profiles are substituted into the conservation equation, which when integrated yields an algebraic expression relating the solution parameters. Recall that the inviscid rollup case did not require an axial momentum balance because Bernoulli's equation applied at all points within the inviscid spiral. Bernoulli's equation no longer applies within the turbulent core because the trailing vortex lines in the wake have become crossed and diffused by the mixing process.

Before proceeding, a special interpretation of the core formation process will be made with respect to the axial momentum balance. First consider the axial momentum balance for purely inviscid rollup. The tapered-cylindrical control volume extends from the wing trailing edge, where the upstream (inlet) face has radius r_{in}, to a location in the wake where rollup is complete, and the downstream (outlet) face has radius r. (See Fig. 5 for an illustration of the turbulent core control volume.) In addition to the pressure forces and momentum fluxes on the inlet and outlet faces, there are axial pressure forces on the tapered streamtube that forms the side of the control volume. The net axial force due to pressure acting on the side can be calculated because the swirl velocity is known and Bernoulli's equation applies on this bounding stream surface.

The result, which depends on the streamtube inlet and outlet radii and not on the detailed shape for small changes, is found by a detailed calculation, which is omitted here. In summary form, the axial momentum balance during the inviscid rollup process is given by

$$\int \underbrace{[p+\rho U_\infty^2]}_{\text{inlet}}\,\mathrm{d}S = \int \underbrace{[p+\rho u^2]}_{\text{inviscid vortex}}\,\mathrm{d}S + \text{side forces} \tag{25}$$

The side forces and the outlet face forces and fluxes are readily calculated from the inviscid solution already obtained. Therefore, the integral of forces and fluxes on the inlet face can be determined from Eq. (25).

A similar momentum balance can be made for the case of turbulent vortex rollup, yielding a similar expression:

$$\int \underbrace{[p+\rho U_\infty^2]}_{\text{inlet}}\,\mathrm{d}S = \int \underbrace{[p+\rho u^2]}_{\text{turbulent vortex}}\,\mathrm{d}S + \text{side forces} \tag{26}$$

The balances represented by Eqs. (25) and (26) share the same integral of inlet conditions at the wing trailing edge. This inlet integral is found from Eq. (25), as mentioned earlier, and analytical expressions are available for the other terms in Eq. (26), which involve unknown turbulent core parameters. Thus, subtracting Eq. (25) from Eq. (26) and neglecting the side force terms, which are approximately equal to each other for small radius changes, gives

$$\int \underbrace{[p+\rho u^2]}_{\text{inviscid vortex}}\,\mathrm{d}S = \int \underbrace{[p+\rho u^2]}_{\text{turbulent vortex}}\,\mathrm{d}S \tag{27}$$

which relates the known axial momentum in a purely inviscid vortex to downstream axial momentum of a turbulent vortex. The advantage of this approach is that streamtube inlet forces and fluxes, which would otherwise require additional modeling, are no longer a factor in the momentum balance.

A physical interpretation of Eq. (27), shown schematically in Fig. 8, is that core formation results from a jump between a supercritical inviscid flow state to a subcritical turbulent flow state. The process is somewhat analogous to a traditional hydraulic jump, which conserves mass flux and axial momentum flux but loses energy in jumping to a subcritical state. This viewpoint also bears a relationship to other work in which vortex jump states have been related to vortex breakdown.[35,36]

In general, the left-hand side of Eq. (27) must be integrated numerically because the inviscid inlet velocity profiles are only known from previous numerical integration of the rollup equations. The portion of the right-hand side of Eq. (27) within the turbulent core can be integrated analytically, because the velocity profiles within the turbulent core are known from Eqs. (18) and (21). Pressure within the turbulent core is calculated by making a radial momentum balance using Eq. (11), which must be integrated over the two swirl velocity regions defined in Eq. (18). Bernoulli's equation applies within the surrounding inviscid spiral and can be used to obtain the reference pressure at the turbulent core boundary. Performing these integrations yields a second relationship between the four solution parameters:

$$\hat{r}_c + \int_0^1 \underbrace{[(\hat{u}(\hat{\xi})^2-1)+\hat{v}(\hat{\xi})^2]\hat{r}(\hat{\xi})\frac{\mathrm{d}\hat{r}}{\mathrm{d}\hat{\xi}}\,\mathrm{d}\hat{\xi}}_{\text{inlet inviscid spiral}}$$

$$= \hat{r}_p + \int_{\hat{\xi}_t}^1 \underbrace{[(\hat{u}(\hat{\xi})^2-1)+\hat{v}(\hat{\xi})^2]\hat{r}(\hat{\xi})\frac{\mathrm{d}\hat{r}}{\mathrm{d}\hat{\xi}}\,\mathrm{d}\hat{\xi}}_{\text{outlet inviscid spiral}}$$

$$+\hat{r}_t^2\left\{\left[(\hat{r}_{\text{in}}(\hat{\xi}_t)/\hat{r}_t)^2-\hat{u}_t\right]^2 G_1(R,m) + 2\hat{u}_t\left[(\hat{r}_{\text{in}}(\hat{\xi}_t)/\hat{r}_t)^2-\hat{u}_t\right]\right.$$

$$\left.-\frac{1}{2}\left(1-\hat{u}_t^2\right)\right\} - (\epsilon\hat{\Gamma}_t)^2 G_2(R) - \epsilon^2\,\ell_\nu\frac{\hat{r}_p}{\hat{r}_c} \tag{28}$$

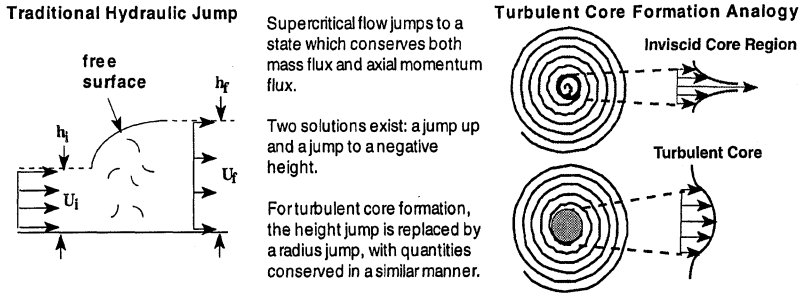

Fig. 8 Hydraulic jump analogy in turbulent core formation.

where two new auxiliary functions, G_1 and G_2, are given by

$$G_1(R,m) \equiv \frac{4(m+2)\{R^{2+m}(m-2)[R^m(m+2)(m-3)+6(m+1)]+12m\}}{3m(m+1)[4+(m-2)R^{2+m}]^2} \tag{29}$$

$$G_2(R) \equiv \frac{9-36\,\ell n R+48(\ell n R)^2-16(\ell n R)^3}{12(1-2\,\ell n R)^2}$$

Again, different assumptions about core velocity profiles will generally produce an equation of the same form as Eq. (28), with different definitions of G_1 and G_2. Note also that in Eq. (28) the two integral terms contain all inviscid spiral quantities expressed parametrically in terms of span location. This matches the form of the inviscid rollup equations, and these integrals are easily evaluated while performing the required shooting procedure.

The final algebraic relationship between the solution parameters is derived from the requirement of continuity of slope in the axial velocity profile at the viscous core boundary. The slope of the viscous core axial velocity profile is found by taking the derivative of the assumed velocity profile, defined in Eq. (21), and evaluating at the turbulent core radius $\hat{r}_t$. The slope of the axial velocity profile in the surrounding inviscid spiral is calculated with the help of the chain rule by dividing Eq. (14) by Eq. (13) and evaluating at the turbulent core radius. The resulting constraint equation is

$$\frac{4(m+2)}{4+(m-2)R^{2+m}}\left[\left(\frac{\hat{r}_{\text{in}}(\hat{\xi}_t)}{\hat{r}_t}\right)^2-\hat{u}_t\right]=\epsilon^2\left(\frac{\mathrm{d}\hat{\Gamma}^2}{\mathrm{d}\hat{\xi}}\Big/\frac{\mathrm{d}\hat{r}_{\text{in}}^2}{\mathrm{d}\hat{\xi}}\right)\Big|_{\hat{\xi}_t} \tag{30}$$

Solution Procedure

The preceding sections outlined the formulation of the conservation equations for the viscous core model. The resulting system consists of four undetermined solution parameters, $\hat{\xi}_t$, $\hat{r}_t$, $\hat{u}_t$, and R; three nonlinear algebraic equations, Eqs. (23), (28), and (30); and a pair of coupled, nonlinear ODEs, Eqs. (13) and (14).

Two of the solution parameters can be determined in closed form, first by solving Eq. (23) for $\hat{u}_t$:

$$\hat{u}_t=\frac{1}{\hat{r}_t^2F_2}\left\{\frac{1}{\hat{\Gamma}_t}\int_0^{\hat{\xi}_t}\hat{\Gamma}(\eta)[\eta-\hat{\bar{\xi}}(\hat{\xi}_t)]\,\mathrm{d}\eta-\hat{r}_{\text{in}}(\hat{\xi}_t)^2F_1\right\} \tag{31}$$

and then eliminating $\hat{u}_t$ between Eqs. (23) and (30) and solving for $\hat{r}_t$:

$$\hat{r}_t=\sqrt{\left(\frac{4(m+2)}{4+(m-2)R^{2+m}}\right)\left\{\hat{r}_{\text{in}}(\hat{\xi}_t)^2(F_1+F_2)-\frac{1}{\hat{\Gamma}_t}\int_0^{\hat{\xi}_t}\hat{\Gamma}(\eta)[\eta-\hat{\bar{\xi}}(\hat{\xi}_t)]\,\mathrm{d}\eta\right\}\Big/\epsilon^2\left(\frac{\mathrm{d}\hat{\Gamma}^2}{\mathrm{d}\hat{\xi}}\Big/\frac{\mathrm{d}\hat{r}_{\text{in}}^2}{\mathrm{d}\hat{\xi}}\right)\Big|_{\hat{\xi}_t}F_2} \tag{32}$$

The two remaining solution parameters, $\hat{\xi}_t$ and R, both lie between 0 and 1 by definition and can be found through the use of an appropriate root-finding technique. Because the axial momentum balance [Eq. (28)] contains two integrals that are evaluated during the shooting procedure, it is necessary to evaluate this equation last.

The solution algorithm requires the following steps. First, for the wing loading distribution of interest, evaluate the left-hand side of Eq. (23) analytically. This term appears in Eqs. (31) and (32). Make initial guesses for R and $\hat{\xi}_t$ (bisection works well), and from these guesses evaluate $\hat{r}_t$ and $\hat{u}_t$ using Eqs. (31) and (32). Numerically integrate Eqs. (13) and (14) with this trial set of initial conditions, adjusting $\hat{\xi}_t$, and with it $\hat{r}_t$ and $\hat{u}_t$, until the axial velocity outer boundary condition is satisfied. Next, evaluate Eq. (28) with the four trial solution parameters. Adjust R and repeat the process until Eq. (28) is satisfied to the desired accuracy. This solution procedure, for a given wing loading distribution and strength, requires approximately 10 s of CPU time on a desktop personal computer.

Because most of the functions are known in closed form, the numerical accuracy of the method is directly related to the tolerance placed on the shooting problem and the axial momentum balance. A fourth-order accurate Runge–Kutta scheme was used for numerical integration of the rollup equations. The results presented here required residuals in the two root-finding procedures to be less than $\mathcal{O}[\epsilon^4]$.

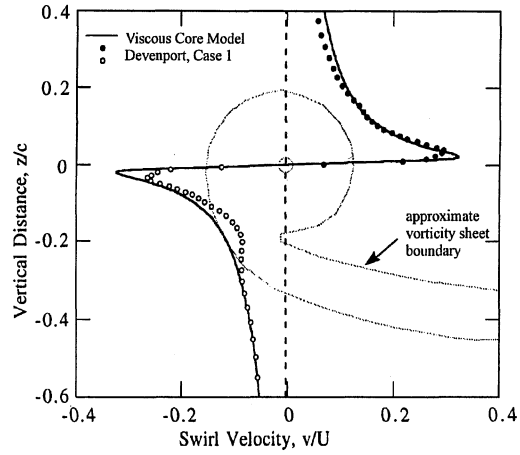

Fig. 9 Comparison of viscous core model swirl velocity prediction with measured vortex data[17]; data were taken along the dashed line.

Results and Discussion

For verification purposes, the viscous vortex model developed here was applied to two configurations that were the subject of recent, comprehensive experimental vortex studies by Devenport et al.[17] and by McAlister and Takahshi.[18] As input, the vortex model required only the wing geometric angle of attack α and aspect ratio AR. With this information and lifting line theory,[37] the theoretical bound circulation was calculated, and from that the appropriate loading-dependent terms in the rollup equations were evaluated. All solutions use the fixed parameter $m=-\frac{2}{3}$ in the assumed axial velocity profiles. This value was found to correlate well with the McAlister and Takahshi axial velocity data.[18] In general, solution parameters were not found to be very sensitive to the particular choice of m.

The first set of results refer to the Devenport et al.[7] study, in which vortex swirl and axial velocity, as well as turbulence stresses and triple products were measured at several stations downstream of a rectangular planform NACA 0012 half-wing with equivalent full-span aspect ratio of 8.66. Reynolds number based on chord was reported as 530,000. A small constant shift (less than the reported uncertainty of the experimental measurements) was applied to the measured vortex swirl data to account for the spanwise velocity of the vortex.

Figure 9 shows the predicted vortex swirl velocity based on the viscous core model, along with experimentally measured values across the vortex five chords downstream of the generating wing. It is clear that the trailing vortex has not yet reached an axisymmetric state. However, the physical structure and orientation of the feeding sheet of trailed vorticity provide insight into the asymmetry in the data. The prediction assumes that the sheet is fully rolled up, when in fact only a fraction of the rollup process is complete at this station. The Betz method applies on a station-by-station basis, which may explain the excellent agreement between measured and predicted swirl velocity on the upper side of the vortex within the sheet boundary. Outside this boundary (in the positive z direction), the measured swirl velocity is less than that predicted by the model, which is consistent with incomplete rollup.

On the lower side of the vortex, the large deviation between predicted and measured swirl velocity corresponds to a gap in vorticity between the coherent, rolled-up core region of the vortex and the concentrated feeding sheet. The approximate sheet boundary

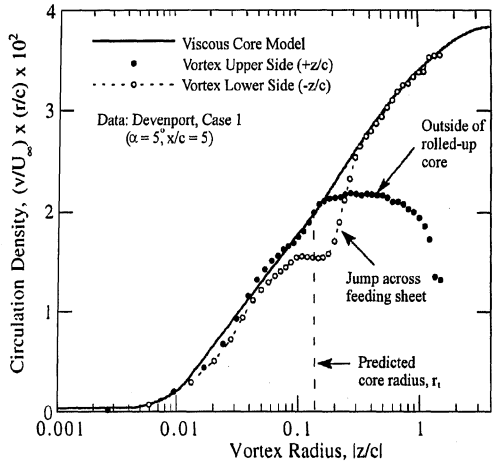

Fig. 10 Comparison of viscous core model circulation density prediction with measured vortex data.[17]

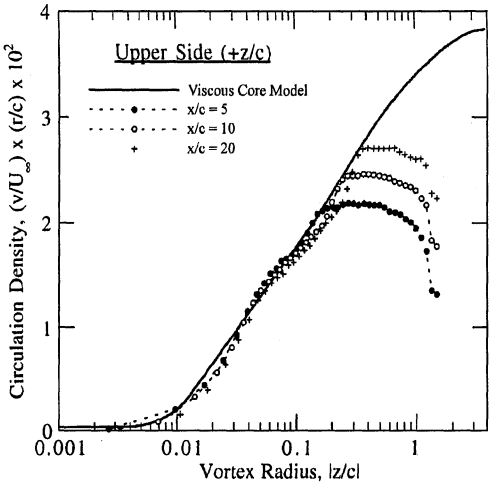

Fig. 11 Growth of circulation density on upper side of vortex.

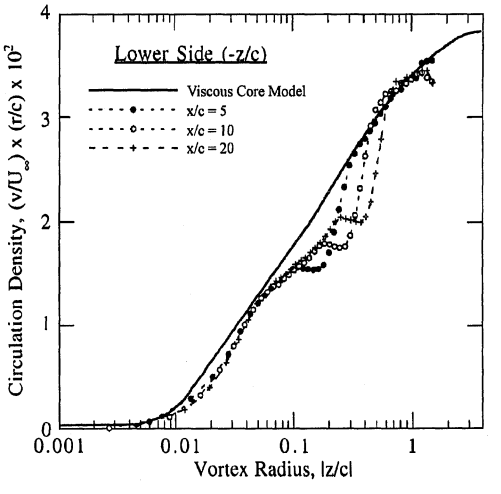

Fig. 12 Growth of circulation density on lower side of vortex.

as reported in Ref. 7 is shown for comparison. This effect is more clearly demonstrated in the circulation distribution across the vortex, as will be shown.

Before proceeding, a special interpretation of vortex circulation will be made that illustrates some important features of vortex formation. The standard definition of circulation entails a line integral around a closed curve,

$$\Gamma = \oint_C \boldsymbol{V} \cdot \mathrm{d}\boldsymbol{s} \tag{33}$$

If the contour is chosen to be a circle of radius r centered at the vortex center, Eq. (33) reduces to

$$\Gamma(r) = \int_0^{2\pi} v_\theta(r, \theta)\, r\, \mathrm{d}\theta \tag{34}$$

For an axisymmetric vortex, the swirl velocity v_θ is a function of r alone, and the circulation at any radius is simply $\Gamma(r) = 2\pi r\, v_\theta(r)$. It is often the case with experimental vortex data that the circulation contour integral must be evaluated from a limited number of points, effectively averaging the values on opposite sides of the core, providing an inaccurate picture of circulation growth in different parts of the vortex. To see this effect, consider a quantity related to the circulation, dubbed here the circulation density,

$$\gamma(r, \theta) \equiv r\, v_\theta(r, \theta) \tag{35}$$

which is the integrand of Eq. (34). For an axisymmetric vortex, the circulation density differs from the circulation only by the constant scale factor 2π and is also equal to the magnitude of the angular momentum per unit mass of the fluid element at that position. For a nonaxisymmetric vortex, the circulation density provides a one-point approximation to the circulation if the vortex were axisymmetric. The assumption here is that the vortex will eventually achieve an axisymmetric structure but is always observed at an intermediate, nonaxisymmetric stage of formation.

Applying the concept of circulation density to the experimental data yields an upper circulation density for measured values in the positive z direction and a lower circulation density for values in the negative z direction. Predicted circulation density, as well as that calculated from the Devenport et al.[17] experimental data, are plotted in Fig. 10. In the rolled-up portion of the core ($|z/c| < 0.1$), measured circulation density is nearly equal in the upper- and lower-halves of the vortex and is well predicted by the viscous core model, implying axisymmetry within the core. The deviation seen around $z/c = 0.02$ corresponds to the area of peak swirl velocity, where the measured data is most affected by vortex wander, a phenomenon discussed in detail in Ref. 17. The primary consequence of wander is to increase the apparent core diameter and decrease the apparent peak swirl velocity of experimental data, each by as much as 30%. The data presented here have not been corrected for wander, which accounts for the slight circulation density mismatch in the core.

Moving outward in the spiral in the negative z direction, a region of constant circulation density is seen, followed by a sharp jump that corresponds to crossing the feeding vorticity sheet. Beyond the sheet boundary, the lower circulation density is very well predicted by the axisymmetric viscous core model.

Moving outward from the core in the opposite ($+z/c$) direction, the upper circulation density is well predicted by the model at small radius until it reaches a maximum, which corresponds to the outermost turn of the rolled-up portion of the sheet. The physical explanation for this is that the vorticity in the feeding sheet has not yet been drawn up and distributed evenly around the vortex. Note in Fig. 10 that the predicted vortex circulation density is directly proportional to the logarithm of radius within the core, as postulated by Hoffman and Joubert.[24] The measured circulation density in this region is not exactly linear, presumably due to wander effects, as already mentioned.

A pair of additional figures confirms the present view of vortex growth and structure. The maximum upper-side circulation density, plotted in Fig. 11 at three downstream stations, is seen to increase with increasing downstream distance. The radius at which the maximum is reached also increases, as additional turns of the original vortex sheet are rolled up into the spiral core. This characteristic radius appears to be proportional to the square root of the downstream distance, which agrees with the overall spiral growth law reported by Devenport et al.[17] In Fig. 12, similar spiral growth is seen in the lower circulation density profile, with the jump across the feeding sheet clearly visible in each case. At all three downstream stations, the circulation beyond the sheet jump is very well predicted by the axisymmetric viscous core model. There is a consistent departure between the predicted and measured values of circulation density, which corresponds to the region between the rolled-up spiral and the remaining feeding sheet. This departure appears to be due to a nonuniform vorticity distribution around the azimuth of the spiral.

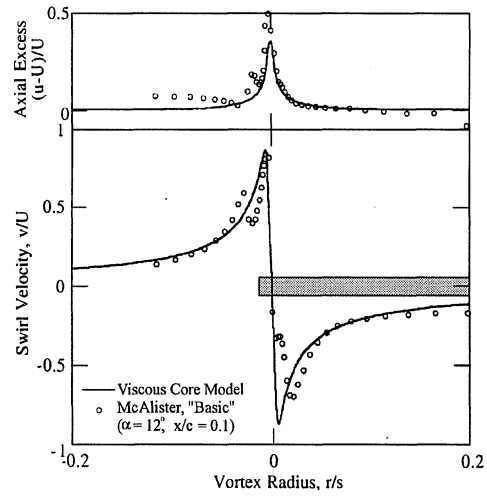

a) $x/c = 0.1$

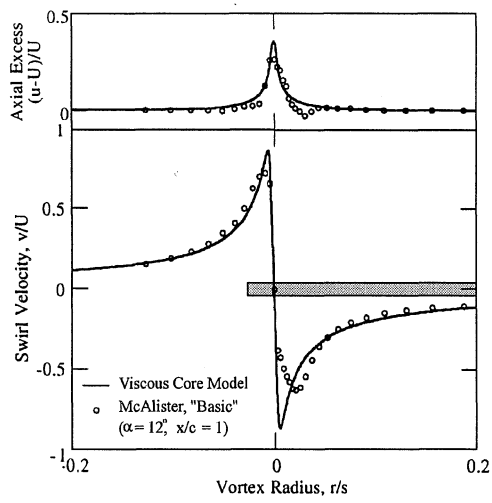

b) $x/c = 4$

Fig. 13 Predicted and measured swirl and axial velocity behind a NACA 0015 half-wing (AR = 6.6 and α = 12).[18]

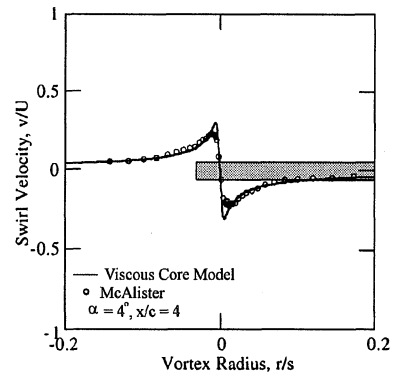

a) $\alpha = 4$

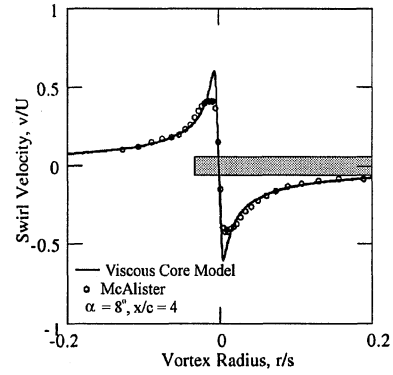

b) $\alpha = 8$

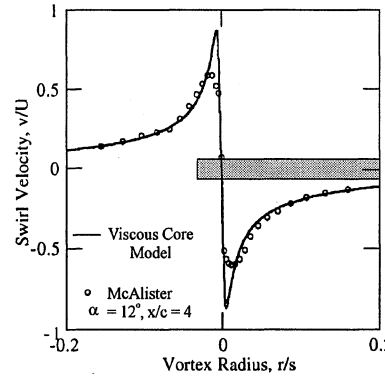

c) $\alpha = 12$

Fig. 14 Predicted and measured swirl velocity behind a NACA 0015 half-wing.[18]

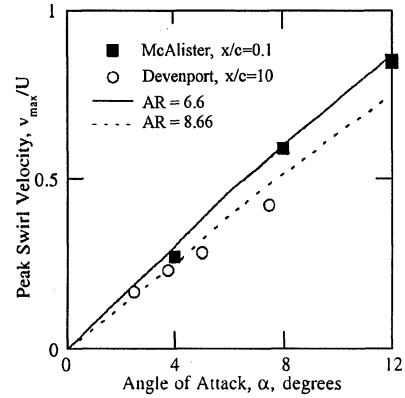

Fig. 15 Predicted and measured peak swirl velocity.

The core growth rate in Figs. 11 and 12 suggests that rollup in the Betz sense will be complete approximately 160 chords downstream, at which point the vortex will be axisymmetric and exhibit the structure predicted by the viscous core model. Of course, after 160 chords, dissipation and decay will also significantly impact the vortex structure.

The second configuration used to verify the viscous core model was a rectangular planform NACA 0015 half-wing with equivalent full-span AR of 6.6, at Reynolds number 1.5×10^6. This study, conducted by McAlister and Takahashi,[18] examined both axial and swirl velocity, as well as wing surface pressure and bound circulation for several half-wings with different ARs at various angles of attack. Figures 13a and 13b show predicted axial and swirl velocity for the basic case at 12-deg angle of attack at two downstream stations. At the first station, only $\frac{1}{10}$th of a chord downstream of the wing trailing edge, the initial measured vortex structure agrees well with that predicted by the viscous core model. Discrete jumps in swirl velocity are evident on both sides of the core, which correspond to jumps across the feeding vortex sheet. Farther downstream, one chord behind the trailing edge, the vortex is approaching an axisymmetric state and shows a reduction in both peak swirl and axial velocity due to viscous decay. These results make a strong case for coupling the viscous core model with an appropriate decay model in future research to accurately predict structure over the life of the vortex.

Figures 14a–14c demonstrate vortex structure as a function of angle of attack α. Seen four chords downstream, the magnitude of peak swirl velocity is linearly proportional to α for both measured and predicted data. Again, the model overpredicts peak swirl velocity, which is in part explained by the effect of vortex wander in the experimental measurements.

The viscous core model provides a simple method for examining trends in solution behavior, such as peak swirl velocity and core size for different loadings and geometries. The following results refer to both the Devenport et al.[17] and McAlister and Takahashi[18] studies. Figure 15 plots the predicted peak swirl velocity as a function of

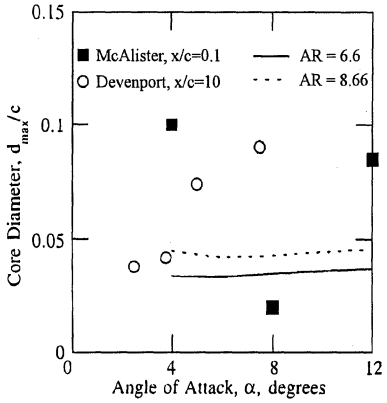

Fig. 16 Predicted and measured peak-to-peak core diameter.

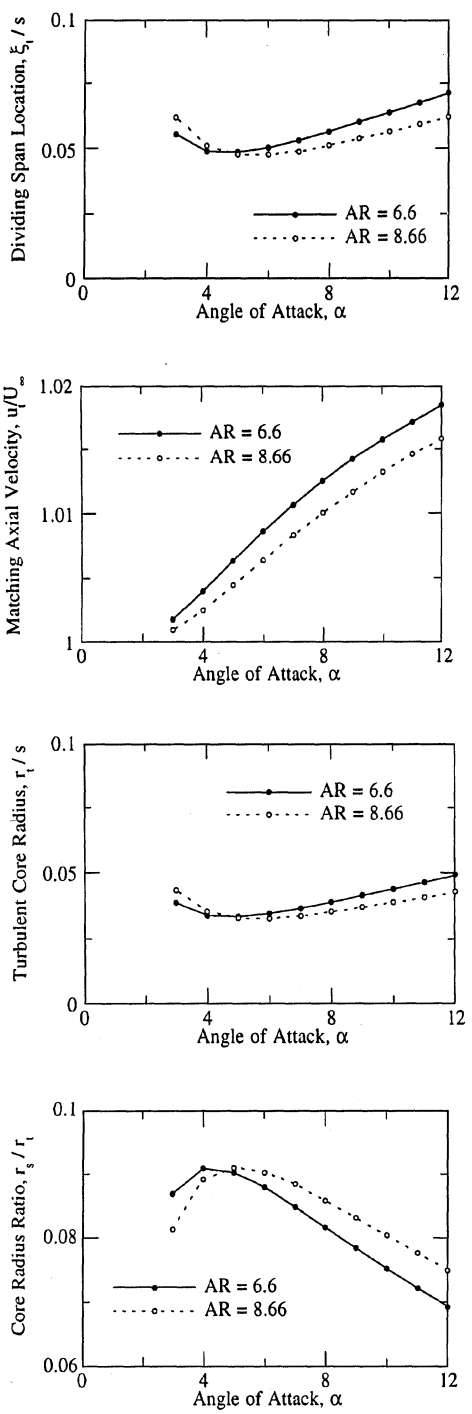

Fig. 17 Viscous core model solution parameters.

angle of attack for the two wing configurations already described. Peak velocities immediately behind the trailing edge of the NACA 0015 wing are well predicted by the model, suggesting that core formation, the hydraulic jump postulated here, is nearly instantaneous. Measured peak velocity 10 cords downstream of the NACA 0012 wing are reasonably predicted by the model, with the overprediction explained by vortex wander.

Peak-to-peak diameter is plotted in Fig. 16. Measured core diameter values for the NACA 0012 wing have been corrected for wander here and demonstrate regular behavior, though the growth trend with increasing angle of attack is not predicted by the model. The data for the NACA 0015 wing do not exhibit any regular trend, and such measurements are likely affected by vortex wander.

Figure 17 shows the solution parameters used to generate the described results. These parameters are found from the viscous core model solution procedure but are considered intermediate steps on the way to generating the preceding vortex velocity profiles.

Conclusions

Results were presented for a new trailing vortex model based on the Betz method for vortex rollup. The model incorporated a differential formulation for inviscid rollup with an integral conservation law model in the viscous core region. The effect of turbulent mixing in the viscous core was handled implicitly through the correct choice of solution velocity functional form. The resulting procedure is computationally efficient and applies to arbitrary wing loading distributions. The model was successfully validated against data from two recent vortex experiments.

Several issues were identified during the model validation process that merit special attention. First, the importance of examining the measured swirl velocity on each side of the vortex, rather than averaging the values was seen. Because vortex models, including the present model, generally assume axisymmetry, it is natural to look for this behavior in both circulation and swirl velocity. However, axisymmetry should be regarded as a steady-state result, with more complex states seen during the formation process. In the present study, such an examination provided new insight into the physics behind trailing vortex spiral growth, confirming the fundamental soundness of the Betz method.

In addition, the importance of modeling vortex decay was recognized due to the fact that the viscous core model consistently overpredicted peak swirl velocity in the core. Some of this overprediction can be attributed to the fact that analytical models are not subject to the effects of vortex wandering. The effect of viscous decay during vortex formation presents an interesting conundrum. On one hand, model predictions immediately downstream of the McAlister and Takahashi wing of Ref. 18 were very good in the core region but became less accurate outside the core because rollup was incomplete. On the other hand, the model appeared on track to give excellent predictions for the Devenport et al.[17] configuration, but it was estimated that this state would be reached far downstream. Coupling decay and dissipation into the present model is an area of ongoing research. An additional effect, which has not been considered here, is viscous blade drag, which will further alter the vortex core structure. A viscous drag model in keeping with the spirit of the viscous core model is already under development as part of the present research program.

Finally, the present model requires some care in the choice of viscous core velocity functions. Based on analysis and experimental observation, the chosen functions were expected to produce reasonable results, which proved to be the case. However, there is still latitude in the choice of different functions. Because core properties are conserved on an integral basis, different combinations of axial and swirl velocity can produce a vortex with the same core radius and peak velocity. Examining the impact of different assumptions on vortex predictions is another area of ongoing research.

Appendix: Starting Solution for the Differential Rollup Equations

As stated in the main text, starting the numerical integration of Eqs. (13) and (14) requires a set of three initial conditions, $\hat{\xi}_i$, $\hat{r}_i$, and $\hat{u}_i$. Because axial velocity is singular exactly at the wing tip, a

more complete solution valid only near the tip is necessary. Near the tip, the circulation is assumed to be given by

$$\Gamma = A\hat{\xi}^q \tag{A1}$$

where, for elliptic loading, $A = \sqrt{2}\Gamma_{\max}$ and $q = \frac{1}{2}$. Assuming that the solutions for $\hat{r}$ and $\hat{u}$ also behave as powers of $\hat{\xi}$, substitution into Eqs. (13) and (14) for elliptic loading gives

$$\hat{r} = (8/27\epsilon)\hat{\xi}^{\frac{3}{2}}, \qquad \hat{u} = (27/8)\epsilon^2\hat{\xi}^{-1} \tag{A2}$$

Unfortunately, Eqs. (A2) provide inadequate starting conditions for the numerical solution of the rollup equations. The problem is that these starting conditions are not of the most general form because they contain no free parameters; a solution starting from these conditions will generally not satisfy the boundary condition $\hat{u} = 1$ at the outer edge of the vortex. To be able to satisfy the outer boundary condition, the solution in the core center must contain an arbitrary constant, which will then be determined by a shooting scheme.

An arbitrary constant is introduced by assuming that the tip solution behaves as a series in unknown powers of $\hat{\xi}$:

$$\hat{u} = \tfrac{27}{8}\epsilon^2\hat{\xi}^{-1} + A_1\hat{\xi}^{\lambda_1} + A_2\hat{\xi}^{\lambda_2} + \cdots \tag{A3}$$

where the lead term has already been determined. That the arbitrary constant does not appear in the lead term is a consequence of the nonlinear nature of these equations. Eliminating $\hat{r}$ between Eqs. (13) and (14) and assuming Γ of the form given by Eq. (A1) yields a second-order, nonlinear ODE for $\hat{u}$:

$$\hat{\xi}\left(\frac{\mathrm{d}\hat{u}^2}{\mathrm{d}\hat{\xi}}\right)^2 - \frac{9}{4}\epsilon^2\hat{u}\left(\frac{\mathrm{d}^2\hat{u}^2}{\mathrm{d}\hat{\xi}^2}\right) = 0 \tag{A4}$$

Substituting Eq. (A3) into Eq. (A4) and collecting terms by power of $\hat{\xi}$ gives

$$A_1\left(\tfrac{27}{8}\epsilon^2\right)^2\tfrac{9}{2}\left(\lambda_1^2 + 3\lambda_1 - 1\right)\hat{\xi}^{-4+\lambda_1} + A_2\mathcal{O}[\hat{\xi}^{-4+\lambda_2}] = 0 \tag{A5}$$

For Eq. (A5) to be valid for all $\hat{\xi}$, either $A_1 = 0$ or $\lambda_1^2 + 3\lambda_1 - 1 = 0$. Because the former does not lead to a general solution form, require the latter condition to hold, which yields $\lambda_1 = (-3 + \sqrt{13})/2$. The positive root was chosen due to the requirement that the powers in the series be monotonically increasing. Factoring out the lead term, the tip solution for axial velocity is now essentially in the form given in Eq. (16). The tip solution for radius is calculated by substituting this series solution for $\hat{u}$ into Eq. (14) and solving for $\hat{r}$.

Additional terms in the tip series can be calculated by repeating the described process, but only the first free constant is necessary to start the numerical integration of the exact rollup equations.

Acknowledgments

This research was sponsored in part by a Graduate Student Researchers Program fellowship from the NASA Ames Research Center, with William Warmbrodt serving as Technical Monitor. The authors would like to thank Kenneth McAlister and William Devenport for providing experimental vortex data.

References

[1]Bilanin, A. J., and Donaldson, C., "Estimation of Velocities and Roll-up in Aircraft Vortex Wakes," *Journal of Aircraft*, Vol. 12, No. 7, 1975, pp. 578–584.

[2]Brown, C. E., "Aerodynamics of Wake Vortices," *AIAA Journal*, Vol. 11, No. 4, 1973, pp. 531–536.

[3]Donaldson, C., Snedeker, R. S., and Sullivan, R. D., "Calculation of Aircraft Wake Velocity Profiles and Comparison with Experimental Measurements," *Journal of Aircraft*, Vol. 11, No. 9, 1974, pp. 547–555.

[4]Donaldson, C., and Bilanin, A. J., "Vortex Wakes of Conventional Aircraft," NATO AGARDograph 204, May 1975, pp. 5–14.

[5]Mason, W. H., and Marchman, J. F., III, "Far-Field Structure of Aircraft Wake Turbulence," *Journal of Aircraft*, Vol. 12, No. 2, 1973, pp. 86–92.

[6]Olsen, J. H., Goldburg, A., and Rogers, M. (eds.), *Aircraft Wake Turbulence and Its Detection*, Plenum, New York, 1971.

[7]Rossow, V. J., "On the Inviscid Rolled-up Structure of Lift Generated Vortices," *Journal of Aircraft*, Vol. 10, No. 11, 1973, pp. 647–650.

[8]Rossow, V. J., Sacco, J. N., Askins, P. A., Bisbee, L. S., and Smith, S. M., "Measurements in 80- by 120-Foot Wind Tunnell of Hazard Posed by Lift-Generated Wakes," AIAA Paper 93-3518, Aug. 1993.

[9]Yates, J. E., "Calculation of Initial Vortex Roll-up in Aircraft Wakes," *Journal of Aircraft*, Vol. 11, No. 7, 1974, pp. 397–400.

[10]Bridgeman, J. O., Ramachandran, K., Caradonna, F. X., and Prichard, D., "The Application of Vorticity Embedding to Parallel Blade-Vortex Interactions," AIAA Paper 94-1919, 1994.

[11]Caradonna, F. X., Strawn, R. C., and Bridgeman, J. O., "An Experimental and Computational Study of Rotor-Vortex Interactions," *Vertica*, Vol. 12, No. 4, 1988, pp. 315–327.

[12]Gallman, J. M., Tung, C., Schultz, K. J., Splettstoesser, W., Buchholz, H., Spiegel, P., Burley, C. L., Brooks, T. E., and Boyd, D. D., Jr., "Effect of Wake Structure on Blade-Vortex Interaction Phenomena: Acoustic Prediction and Validation," AIAA 16th Aeroacoustics Conf., Munich, Germany, June 1995.

[13]Martin, R. M., Marcolini, M. A., Splettsoesser, W. R., and Schultz, K. J., "Wake Geometry Effects on Rotor Blade-Vortex Interaction Noise Directivity," NASA TP-3015, Nov. 1990.

[14]McCroskey, W. J., "Vortex Wakes of Rotorcraft," AIAA Paper 95-0530, Jan. 1995.

[15]Srinivasan, G. R., McCroskey, W. J., and Baeder, J. D., "Aerodynamics of Two-Dimensional Blade-Vortex Interaction," *AIAA Journal*, Vol. 24, No. 10, 1986, pp. 1569–1576.

[16]Yu, Y. H., Tung, C., Gallman, J. M., Splettstoesser, W. R., Schultz, K. J., van der Wall, B., Spiegel, P., Rahier, G., Michea, B., and Costes, M., "Aerodynamics and Acoustics of Rotor Blade–Vortex Interactions: Analysis Capability and Its Validation," AIAA Paper 93-4332, Oct. 1993.

[17]Devenport, W. J., Rife, M. C., Liapis, S. I., and Follin, G. J., "The Structure and Development of a Wing-Tip Vortex," *Journal of Fluid Mechanics*, Vol. 312, April 1996, pp. 67–106.

[18]McAlister, K. W., and Takahashi, R. K., "NACA 0015 Wing Pressure and Trailing Vortex Measurements," NASA TP-3151, Nov. 1991.

[19]Chow, J. S., Zilliac, G. G., and Bradshaw, P., "Measurements in the Near-Field of a Turbulent Wingtip Vortex," AIAA Paper 93-0551, Jan. 1993.

[20]Tung, C., Pucci, S. L., Caradonna, F. X., and Morse, H. A., "The Structure of Trailing Vortices Generated by Model Rotor Blades," *Vertica*, Vol. 7, No. 1, 1983, pp. 33–43.

[21]Chigier, N. A., and Corsiglia, V. R., "Wind-Tunnel Studies of Wing Wake Turbulence," *Journal of Aircraft*, Vol. 9, 1972, pp. 820–825.

[22]Corsiglia, V. R., Schwind, R. G., and Chigier, N. A., "Rapid Scanning, Three-Dimensional Hot-Wire Anemometer Surveys of Wing-Tip Vortices," *Journal of Aircraft*, Vol. 10, No. 12, 1973, pp. 752–757.

[23]El-Ramly, Z., and Rainbird, W. J., "Flow Survey of the Vortex Wake Behind Wings," *Journal of Aircraft*, Vol. 14, No. 11, 1977, pp. 1102–1108.

[24]Hoffmann, E. R., and Joubert, P. N., "Turbulent Line Vortices," *Journal of Fluid Mechanics*, Vol. 16, 1963, pp. 395–411.

[25]Orloff, K. L., "Trailing Vortex Wind-Tunnel Diagnostics with a Laser Velocimeter," *Journal of Aircraft*, Vol. 11, No. 8, 1974, pp. 477–482.

[26]Dacles-Mariani, J., Rogers, S., Kwak, D., Zilliac, G., and Chow, J., "A Computational Study of Wingtip Vortex Flowfield," AIAA Paper 93-3010, July 1993.

[27]Moore, D. W., "A Numerical Study of the Roll-up of a Finite Vortex Sheet," *Journal of Fluid Mechanics*, Vol. 63, No. 2, 1974, pp. 225–235.

[28]Srinivasan, G. R., McCroskey, W. J., Baeder, J. D., and Edwards, T. A., "Numerical Solution of Tip Vortices of Wings in Subsonic and Transonic Flows," *AIAA Journal*, Vol. 26, No. 10, 1988, pp. 1153–1162.

[29]Betz, A., "Behavior of Vortex Systems," TR, NACA TM-713, June 1933.

[30]Bliss, D. B., "Prediction of Tip Vortex Self-Induced Parameters in Terms of Rotor Blade Loading," American Helicopter Society National Specialists Meeting on Aerodynamics and Aeroacoustics, Session Aerodynamics 2, Paper 5, Arlington, TX, 1987.

[31]Scully, M. P., "Computation of Helicopter Rotor Wake Geometry and Its Influence on Rotor Harmonic Loads," Massachusetts Inst. of Technology, ASRL TR-178-1, Cambridge, MA, March 1975.

[32]Batchelor, G. K., "Axial Flow in Trailing Line Vortices," *Journal of Fluid Mechanics*, Vol. 20, No. 4, 1964, pp. 645–658.

[33]Schlichting, H., *Boundary Layer Theory*, McGraw–Hill, New York, 1951, Chap. 10.

[34]McCormick, B. W., Tangler, J. L., and Sherrieb, H. E., "Structure of Trailing Vortices," *Journal of Aircraft*, Vol. 5, No. 3, 1968, pp. 260–267.

[35]Benjamin, T. B., "Theory of Vortex Breakdown," *Journal of Fluid Mechanics*, Vol. 14, Pt. 4, 1962, pp. 593–629.

[36]Landahl, M. T., and Widnall, S. E., "Vortex Control," *Aircraft Wake Turbulence and Its Detection*, edited by J. Olsen, A. Goldberg, and M. Rogers, Plenum, New York, 1971, pp. 137–155.

[37]Anderson, J. D., Jr., *Fundamentals of Aerodynamics*, 2nd ed., McGraw–Hill, New York, 1991, Sec. 5.3.

A. Plotkin
Associate Editor